Mechanical Systems and Signal Processing 102 (2018) 87–101

Contents lists available at ScienceDirect

Mechanical Systems and Signal Processing

journal homepage: www.elsevier.com/locate/ymssp

An energy-optimal solution for transportation control of cranes with double pendulum dynamics: Design and experiments

Ning Sun *, Yiming Wu, He Chen, Yongchun Fang *

Institute of Robotics and Automatic Information Systems (IRAIS), Nankai University, Tianjin, China
Tianjin Key Laboratory of Intelligent Robotics (tjKLIR), Nankai University, Tianjin, China

ARTICLE INFO

Article history:
Received 14 June 2017
Received in revised form 24 August 2017
Accepted 16 September 2017
Available online 22 September 2017

Keywords:
Underactuated systems
Double pendulum cranes
Energy consumption
Swing elimination

ABSTRACT

Underactuated cranes play an important role in modern industry. Specifically, in most situations of practical applications, crane systems exhibit significant double pendulum characteristics, which makes the control problem quite challenging. Moreover, most existing planners/controllers obtained with standard methods/techniques for double pendulum cranes cannot minimize the energy consumption when fulfilling the transportation tasks. Therefore, from a practical perspective, this paper proposes an energy-optimal solution for transportation control of double pendulum cranes. By applying the presented approach, the transportation objective, including fast trolley positioning and swing elimination, is achieved with minimized energy consumption, and the residual oscillations are suppressed effectively with all the state constrains being satisfied during the entire transportation process. As far as we know, this is the *first* energy-optimal solution for transportation control of underactuated double pendulum cranes with various state and control constraints. Hardware experimental results are included to verify the effectiveness of the proposed approach, whose superior performance is reflected by being experimentally compared with some comparative controllers.

1. Introduction

Mechatronic systems have been widely applied in modern industrial fields, and the issues of dynamic analysis and control for such systems have been studied both theoretically and practically [1–3]. In particular, with numerous merits such as high flexibility, low energy consumption, low production costs, simple mechanical structure, and so on, underactuated mechatronic systems have attracted more interests in academia [4–14]. The fact that the number of independent control inputs is less than the degrees of freedom makes the control problem for underactuated systems still challenging and deserve further studies both theoretically and practically.

Underactuated overhead cranes are now widely used in industrial applications. Over the past decades, many ambitious control strategies for overhead crane systems have been reported in the literature [15–39]. Specifically, Rami et al. present a comprehensive review of crane control strategies in [15] which discusses the latest research works. In [16], a novel nonlinear controller for overhead cranes is presented by combining the partial feedback linearization method and the sliding mode technique. In [17], a Lyapunov-based adaptive controller is designed to suppress the undesirable residual swings of cranes with boundary output constraints. Ref. [18] exploits a robust error tracking control method for overhead crane systems

* Corresponding authors at: Institute of Robotics and Automatic Information System (IRAIS), Nankai University, Tianjin, China.
E-mail addresses: sunn@nankai.edu.cn (N. Sun), fangyc@nankai.edu.cn (Y. Fang).

http://dx.doi.org/10.1016/j.ymssp.2017.09.027
0888-3270/

which pre-specifies the error trajectories of the trolley and the payload swing. Ref. [19] applies the differential-flatness-based approach to the finite-time regulation controller for underactuated crane systems. Moreover, some sliding-mode-based controller are presented [20–22]. For example, a sliding-mode antiswing controller is proposed for overhead cranes, which guarantees asymptotic stability while keeping all state signals bounded [21]. Refs. [23–25] suggest some energy analysis-based controllers for underactuated crane systems. In addition, some intelligent algorithms are also introduced to enhance the control performance, such as learning control methods [26], fuzzy control methods [27–29], model predictive control methods [30], and neural network based controllers [31,32]. Then, trajectory planning methods are designed based on the coupling behavior existing between the translational movement and the payload swing [33–35]. For example, in [33], Sun et al. propose a phase plane based trajectory planning method, in which a three segment trajectory is obtained by geometric analysis, which can achieve the dual objective of swing suppression and residual swing elimination. Moreover, the input shaping methods are also applied to crane systems in [36–39] which realize residual swing suppression and state tracking. It is worthwhile to mention that, most existing approaches assume the hook and the payload as a mass point. Then the structure of the overhead crane system can be reduced into a single pendulum model, for which the control objective is usually aimed at achieving accurate orientation when transporting the payload. The payload (traditionally heavy cargo) is connected to the trolley through a rope and a hook. Thus, it will be very dangerous if the payload swings back and forth during the transportation process. In most cases, cranes are operated by skilled technicians. However, when cranes are manually manipulated, mistakes are usually unavoidable and payloads often exhibit uncontrolled residual oscillations, which are very likely to trigger serious accidents. Therefore, high performance control of overhead cranes for overhead crane systems has significant importance and is worthy of further studies.

In fact, in most situations, the mass of the hook is large and cannot be neglected. Moreover, the centers of gravity of the hook and the payload do not coincide with each other. This makes the system present significant double pendulum characteristics. On this occasion, the planners/controllers designed based upon traditional single pendulum representation are not suitable. Up to now, the research of double pendulum cranes is still at an early stage and there are many unresolved problems [40–49]. For example, In [40], an adaptive tracking controller for double pendulum cranes subject to parametric uncertainties and external disturbances is proposed, which guarantees that the trolley tracking error is within a prior set of boundary conditions and converges to zero rapidly. The input shaping technology is also applied to double pendulum crane systems [41–45] to suppress the oscillatory dynamics. In [46], one conventional sliding mode controller and one hierarchical sliding mode controller are designed to achieve transportation and anti-swing control objectives for double pendulum crane systems, both of which are discontinuous full state feedback controllers. Several intelligent controllers are proposed and used in [47,48]. More recently, in [49], an amplitude-saturated output feedback antiswing controller is proposed to regulate double pendulum cranes. However, none of the existing planners/controllers for double pendulum cranes take consideration of energy consumption which is an important criterion in modern industry.

To remedy the drawbacks of the state-of-art studies and to realize the energy optimal objective, this paper proposes an off-line energy-optimal trajectory planner for the horizontal motion control of double pendulum crane systems with the consideration of state constraints. In [35], Wu et al. propose an energy-optimal planner to reduce the energy consumption for single pendulum crane systems. In this paper, an energy-optimal solution is *firstly* presented for double pendulum cranes to move the trolley to the desired location and eliminate the double pendulum angle swings while minimizing energy consumption and keeping all the state variables within the given boundaries for safety concern. It is worthwhile to mention that the proposed planner generates the energy-optimal trajectory offline by implementing the optimization algorithm before practical use. Specifically, we first provide the system dynamics by using Lagrange's method. After that, the energy consumption function is constructed based on the dynamics. Then, after the convexification of the energy consumption function (through some transformations and calculations) and the discretization of the overall system (including the system dynamics, the initial/final conditions, the energy consumption function, and the preset state constraints), the control problem is formulated as a quadratic programming (QP) problem. Then the convex optimization technique is applied to solve the presented QP problem. Finally, hardware experiments are implemented on a double pendulum crane testbed to verify the performance of the proposed planner.

Compared with the existing planners/controllers, the merits of the suggested approach can be summarized as follows:

- The presented planner *firstly* solves the energy-optimal control problem for double pendulum cranes.
- System state constraints are taken into consideration to ensure that, all the system state variables are kept within given scopes during the entire process. Meanwhile, theoretically, there is no residual swing when the trolley reaches the destination.
- Hardware experiments are implemented on a double pendulum crane testbed, which are more convincing than merely simulation results provided by most existing works on double pendulum cranes.

The rest of this paper is arranged as follows. Section 2 provides the system dynamics of the double pendulum cranes system. Section 3 states the energy-optimal trajectory planning problem. The problem is formulated with initial/final conditions, energy consumption, and preset state constraints. Section 4 reformulates the energy-optimal trajectory planning issue into a convexity-based QP problem by discretizing the system dynamics. In Section 5, both numerical simulation and hardware experimental results are given to illustrate the satisfactory control performance of the proposed approach. Section 6 summarizes the main results of the paper.

2. System dynamics

The schematic diagram of double pendulum cranes is shown in Fig. 1. The underactuated double pendulum crane system can be described with the following dynamics [49]:

$$(M+m_1+m_2)\ddot{x}+(m_1+m_2)l_1(\cos\theta_1\ddot{\theta}_1-\dot{\theta}_1^2\sin\theta_1)+m_2l_2\ddot{\theta}_2\cos\theta_2-m_2l_2\dot{\theta}_2^2\sin\theta_2=F, \tag{1}$$

$$(m_1+m_2)l_1\cos\theta_1\ddot{x}+(m_1+m_2)l_1^2\ddot{\theta}_1+m_2l_1l_2\cos(\theta_1-\theta_2)\ddot{\theta}_2+m_2l_1l_2\sin(\theta_1-\theta_2)\dot{\theta}_2^2+(m_1+m_2)gl_1\sin\theta_1+d_1\dot{\theta}_1=0, \tag{2}$$

$$m_2l_2\cos\theta_2\ddot{x}+m_2l_1l_2\cos(\theta_1-\theta_2)\ddot{\theta}_1+m_2l_2^2\ddot{\theta}_2-m_2l_1l_2\dot{\theta}_1^2\sin(\theta_1-\theta_2)+m_2gl_2\sin\theta_2+d_2\dot{\theta}_2=0, \tag{3}$$

where the definitions of the system state variables and parameters in (1)–(3) are shown in Table 1 in details.

For practical applications, the following approximations are usually valid for cranes [34,35,41,44,45][1]: $\sin\theta_1\approx\theta_1,\sin\theta_2\approx\theta_2,\cos\theta_1\approx1,\cos\theta_2\approx1,\sin(\theta_1-\theta_2)\approx\theta_1-\theta_2,\cos(\theta_1-\theta_2)\approx1,\dot{\theta}_1^2\approx0,\dot{\theta}_2^2\approx0$. Then, we can rewrite (1)–(3) as follows:

$$(M+m_1+m_2)\ddot{x}+(m_1+m_2)l_1\ddot{\theta}_1+m_2l_2\ddot{\theta}_2=F, \tag{4}$$

$$\ddot{x}+l_1\ddot{\theta}_1+\frac{m_2l_2}{m_1+m_2}\cdot\ddot{\theta}_2+g\theta_1+\frac{d_1}{(m_1+m_2)l_1}\dot{\theta}_1=0, \tag{5}$$

$$\ddot{x}+l_1\ddot{\theta}_1+l_2\ddot{\theta}_2+g\theta_2+\frac{d_2}{m_2l_2}\dot{\theta}_2=0. \tag{6}$$

The equations in (5) and (6) reflect the coupling relationship between the trolley acceleration and double pendulum angle swings, i.e., they fully reveal how the trolley movement affects the swing motions. Hence, they are the basis of the subsequent trajectory (motion) planning analysis. Then, after some arrangements, (5) and (6) can be rewritten into

$$\ddot{\theta}_1=-\frac{\ddot{x}}{l_1}-\frac{(m_1+m_2)g}{m_1l_1}\cdot\theta_1+\frac{m_2g}{m_1l_1}\cdot\theta_2-\frac{d_1}{m_1l_1^2}\cdot\dot{\theta}_1+\frac{d_2}{m_1l_1l_2}\cdot\dot{\theta}_2, \tag{7}$$

$$\ddot{\theta}_2=\frac{(m_1+m_2)g}{m_1l_2}\cdot\theta_1-\frac{(m_1+m_2)g}{m_1l_2}\cdot\theta_2+\frac{d_1}{m_1l_1l_2}\cdot\dot{\theta}_1-\frac{(m_1+m_2)d_2}{m_1m_2l_2^2}\cdot\dot{\theta}_2. \tag{8}$$

The translational acceleration $\ddot{x}(t)$ can be viewed as the new input $u(t)$, and then (7) and (8) can be rewritten into the following state-space form:

$$\dot{\boldsymbol{\chi}}=A\boldsymbol{\chi}+Bu, \tag{9}$$

where $\boldsymbol{\chi}(t)$ denotes the system state vector with the following definition:

$$\boldsymbol{\chi}=\left[x,\quad \dot{x},\quad \theta_1,\quad \dot{\theta}_1,\quad \theta_2,\quad \dot{\theta}_2\right]^\top. \tag{10}$$

A,B are matrices defined as follows:

$$A=\begin{bmatrix}0, & 1, & 0, & 0, & 0, & 0\\ 0, & 0, & 0, & 0, & 0, & 0\\ 0, & 0, & 0, & 1, & 0, & 0\\ 0, & 0, & a_{43}, & a_{44}, & a_{45}, & a_{46}\\ 0, & 0, & 0, & 0, & 0, & 1\\ 0, & 0, & a_{63}, & a_{64}, & a_{65}, & a_{66}\end{bmatrix}, \tag{11}$$

$$B=\left[0,\quad 1,\quad 0,\quad -\tfrac{1}{l_1},\quad 0,\quad 0\right]^\top, \tag{12}$$

where the matric parameters a_{ij}'s, $i=4,6,\ j=3,4,5,6$ are defined for simplicity as follows:

$$a_{43}=-\frac{(m_1+m_2)g}{m_1l_1},\quad a_{44}=-\frac{d_1}{m_1l_1^2},\quad a_{45}=\frac{m_2g}{m_1l_1},\quad a_{46}=\frac{d_2}{m_1l_1l_2},$$
$$a_{63}=\frac{(m_1+m_2)g}{m_1l_2},\quad a_{64}=\frac{d_1}{m_1l_2l_1},\quad a_{65}=-\frac{(m_1+m_2)g}{m_1l_2},\quad a_{66}=-\frac{(m_1+m_2)d_2}{m_1m_2l_2^2}.$$

[1] As will be shown later, the proposed planner can ensure that the swing angles $\theta_1(t),\theta_2(t)$ are of small values, so that the approximations are theoretically valid, too.

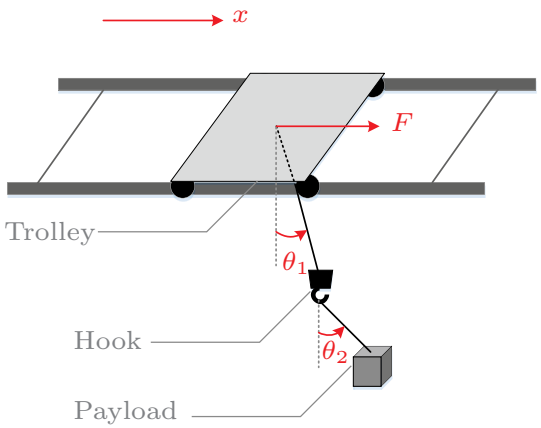

Fig. 1. The schematic diagram of double pendulum cranes.

In this paper, the initial time and the final time are assumed to be $t = 0$ and $t = t_f$ (t_f is a preset value). Therefore, the initial and final conditions can be depicted respectively as follows:

$$\begin{aligned}\boldsymbol{\chi}(0) &= [\,x_0, \quad \dot{x}_0, \quad \theta_{10}, \quad \dot{\theta}_{10}, \quad \theta_{20}, \quad \dot{\theta}_{20}\,]^\top \\ &= [\,0, \quad 0, \quad 0, \quad 0, \quad 0, \quad 0\,]^\top, \end{aligned} \tag{13}$$

$$\begin{aligned}\boldsymbol{\chi}(k_f) &= [\,x_f, \quad \dot{x}_f, \quad \theta_{1f}, \quad \dot{\theta}_{1f}, \quad \theta_{2f}, \quad \dot{\theta}_{2f}\,]^\top \\ &= [\,x_f, \quad 0, \quad 0, \quad 0, \quad 0, \quad 0\,]^\top, \end{aligned} \tag{14}$$

where x_f represents the final translational displacement of the trolley.

3. Problem formulation

Because there usually exist physical constraints in practice, the velocity and acceleration of the crane system should be restricted to certain extents. In addition, for safety reasons, the amplitudes of the angle swings should also be restricted within allowable scopes. In this paper, the upper bounds of the velocity, acceleration, and angles are constrained as follows:

$$\begin{aligned} &|\dot{x}(t)| \leqslant v_{\max}, \quad |\ddot{x}(t)| \leqslant a_{\max}, \\ &|\theta_1(t)| \leqslant \theta_{1\max}, \quad |\theta_2(t)| \leqslant \theta_{2\max}, \\ &|\dot{\theta}_1(t)| \leqslant \theta_{1v\max}, \quad |\dot{\theta}_2(t)| \leqslant \theta_{2v\max}, \end{aligned} \tag{15}$$

where $v_{\max}, a_{\max}$ represent the allowable constraints of the translational velocity and acceleration, $\theta_{1\max}, \theta_{2\max}, \theta_{1v\max}$, and $\theta_{2v\max}$ denote the preset limitations of the angle swings and the corresponding velocities for safety.

The objective is to realize an energy-optimal control of double pendulum cranes, considering the total energy consumption J of the double pendulum crane system expressed as follows:

$$J = \int_0^{t_f} F\dot{x}\,\mathrm{d}t, \tag{16}$$

and then the control problem can be formulated as follows:

Table 1
Parameters and state variables.

Parameters	Physical significance	Units
M	Mass of the trolley	kg
m_1, m_2	Mass of the hook and the payload	kg
l_1	Length of the rope	m
l_2	Distance between the center of hook and the payload	m
$x(t)$	Translational displacement of the trolley	m
$\theta_1(t)$	Swing angle of the hook with respect to the vertical axis	rad
$\theta_2(t)$	Swing angle of the payload with respect to the vertical axis	rad
$F(t)$	Resultant force applied to the trolley	N
d_1, d_2	Constant damping coefficients	

$$\begin{aligned}
&\text{minimize } J = \int_0^{t_f} F\dot{x}\mathrm{d}t,\\
&\quad \text{s.t. } \dot{\boldsymbol{\chi}} = A\boldsymbol{\chi} + Bu,\\
&\qquad \boldsymbol{\chi}(0) = [0,\ \ 0,\ \ 0,\ \ 0,\ \ 0,\ \ 0]^\top,\\
&\qquad \boldsymbol{\chi}(k_f) = [x_f,\ \ 0,\ \ 0,\ \ 0,\ \ 0,\ \ 0]^\top,\\
&\qquad |\dot{x}(t)| \leqslant v_{\max}, |\ddot{x}(t)| \leqslant a_{\max},\\
&\qquad |\theta_1(t)| \leqslant \theta_{1\max}, |\theta_2(t)| \leqslant \theta_{2\max},\\
&\qquad |\dot{\theta}_1(t)| \leqslant \theta_{1v\max}, |\dot{\theta}_2(t)| \leqslant \theta_{2v\max}.
\end{aligned} \tag{17}$$

However, the problem presented in (17) is difficult to solve directly since it is a non-convex problem. Subsequently, we will first *convert* (17) into an easy-to-solve convex optimization problem, and then suggest a QP based energy-optimal solution for the double pendulum crane systems in the presence of state constraints.

4. Convexity-based energy-optimal planning

In this section, the to-be-solved problem, stated in (17), will be reformulated into a QP problem, and after dynamics discretization, a convexity-based energy-optimal trajectory planner will be presented.

First, by letting τ be the sampling time, we can obtain the corresponding discrete-time system dynamics as

$$\boldsymbol{\chi}(k+1) = H\boldsymbol{\chi}(k) + \boldsymbol{G}u(k), \tag{18}$$

where $H \in \mathbb{R}^{6\times 6}$ and $\boldsymbol{G} \in \mathbb{R}^{6\times 1}$ are the discrete-time state matrices defined as

$$H = e^{A\tau}, \quad \boldsymbol{G} = \int_0^{\tau} e^{At}B\,\mathrm{d}t. \tag{19}$$

By treating $\boldsymbol{\chi}(0)$ and $u(k)$ as the initial state and the system input, the solution of (18) can be obtained as follows:

$$\boldsymbol{\chi}(k) = H^k\boldsymbol{\chi}(0) + \sum_{j=0}^{k-1} H^{k-j-1}\boldsymbol{G}u(j). \tag{20}$$

By letting k_f be the final sampling instant, the system state and input sequence are given as

$$\begin{aligned}
\bar{\boldsymbol{\chi}} &:= [\boldsymbol{\chi}^\top(1), \boldsymbol{\chi}^\top(2), \ldots, \boldsymbol{\chi}^\top(k_f)]^\top,\\
\bar{\boldsymbol{u}} &:= [u(0), u(1), \ldots, u(k_f-1)]^\top.
\end{aligned}$$

Then, from (20), the state sequence can be written as

$$\bar{\boldsymbol{\chi}} = P\boldsymbol{\chi}(0) + Q\bar{\boldsymbol{u}}, \tag{21}$$

where $P \in \mathbb{R}^{6k_f\times 6}$ and $Q \in \mathbb{R}^{6k_f\times k_f}$ are matrices with the following definitions:

$$P = \begin{bmatrix} H^1, & H^2, & \ldots, & H^{k_f} \end{bmatrix}^\top, \tag{22}$$

$$Q = \begin{bmatrix} H^0\boldsymbol{G} & & & \\ H^1\boldsymbol{G}, & H^0\boldsymbol{G} & & \\ \vdots & \vdots & \ddots & \\ H^{k_f-1}\boldsymbol{G}, & H^{k_f-2}\boldsymbol{G}, & \cdots, & H^0\boldsymbol{G} \end{bmatrix}. \tag{23}$$

It is also shown from (21) that once we know a certain input sequence, the corresponding state sequence will then be obtained.

Next, together with (10) and (21), the following angular and velocity sequences:

$$\begin{aligned}
\boldsymbol{\theta}_1 &:= [\theta_1(1), \theta_1(2), \ldots, \theta_1(k_f)]^\top,\\
\boldsymbol{\theta}_2 &:= [\theta_2(1), \theta_2(2), \ldots, \theta_2(k_f)]^\top,\\
\dot{\boldsymbol{x}} &:= [\dot{x}(1), \dot{x}(2), \ldots, \dot{x}(k_f)]^\top,\\
\dot{\boldsymbol{\theta}}_1 &:= [\dot{\theta}_1(1), \dot{\theta}_1(2), \ldots, \dot{\theta}_1(k_f)]^\top,\\
\dot{\boldsymbol{\theta}}_2 &:= [\dot{\theta}_2(1), \dot{\theta}_2(2), \ldots, \dot{\theta}_2(k_f)]^\top,
\end{aligned}$$

and the acceleration sequences $\ddot{\boldsymbol{x}}$ can be transformed into the following form with respect to the input sequence $\bar{\boldsymbol{u}}$:

$$\boldsymbol{\theta}_1 := \Omega_{\theta_1}\bar{\boldsymbol{\chi}} = \Omega_{\theta_1}P\boldsymbol{\chi}(0) + \Omega_{\theta_1}Q\bar{\boldsymbol{u}}, \tag{24}$$

$$\boldsymbol{\theta}_2 := \Omega_{\theta_2}\bar{\boldsymbol{\chi}} = \Omega_{\theta_2}P\boldsymbol{\chi}(0) + \Omega_{\theta_2}Q\bar{\boldsymbol{u}}, \tag{25}$$
$$\dot{\boldsymbol{x}} = \Omega_{vx}\bar{\boldsymbol{\chi}} = \Omega_{vx}P\boldsymbol{\chi}(0) + \Omega_{vx}Q\bar{\boldsymbol{u}}, \tag{26}$$
$$\dot{\boldsymbol{\theta}}_1 = \Omega_{v\theta_1}\bar{\boldsymbol{\chi}} = \Omega_{v\theta_1}P\boldsymbol{\chi}(0) + \Omega_{v\theta_1}Q\bar{\boldsymbol{u}}, \tag{27}$$
$$\dot{\boldsymbol{\theta}}_2 = \Omega_{v\theta_2}\bar{\boldsymbol{\chi}} = \Omega_{v\theta_2}P\boldsymbol{\chi}(0) + \Omega_{v\theta_2}Q\bar{\boldsymbol{u}}, \tag{28}$$
$$\ddot{\boldsymbol{x}} = I_{k_f}\bar{\boldsymbol{u}}, \tag{29}$$

where I_{k_f} is an identity matrix and $\Omega_{\theta_1}, \Omega_{\theta_2}, \Omega_{vx}, \Omega_{v\theta_1}, \Omega_{v\theta_2} \in \mathbb{R}^{k_f \times 6k_f}$ are matrices given as

$$\begin{aligned}
\Omega_{\theta_1} &= \mathrm{diag}\{\boldsymbol{\Phi}_{\theta_1}, \quad \boldsymbol{\Phi}_{\theta_1}, \quad \cdots, \quad \boldsymbol{\Phi}_{\theta_1}\},\\
\Omega_{\theta_2} &= \mathrm{diag}\{\boldsymbol{\Phi}_{\theta_2}, \quad \boldsymbol{\Phi}_{\theta_2}, \quad \cdots, \quad \boldsymbol{\Phi}_{\theta_2}\},\\
\Omega_{vx} &= \mathrm{diag}\{\boldsymbol{\Phi}_{vx}, \quad \boldsymbol{\Phi}_{vx}, \quad \cdots, \quad \boldsymbol{\Phi}_{vx}\},\\
\Omega_{v\theta_1} &= \mathrm{diag}\{\boldsymbol{\Phi}_{v\theta_1}, \quad \boldsymbol{\Phi}_{v\theta_1}, \quad \cdots, \quad \boldsymbol{\Phi}_{v\theta_1}\},\\
\Omega_{v\theta_2} &= \mathrm{diag}\{\boldsymbol{\Phi}_{v\theta_2}, \quad \boldsymbol{\Phi}_{v\theta_2}, \quad \cdots, \quad \boldsymbol{\Phi}_{v\theta_2}\},
\end{aligned}$$

with $\boldsymbol{\Phi}_{\theta_1}, \boldsymbol{\Phi}_{\theta_2}, \boldsymbol{\Phi}_{vx}, \boldsymbol{\Phi}_{v\theta_1}, \boldsymbol{\Phi}_{v\theta_2} \in \mathbb{R}^{1\times 6}$ being defined as

$$\begin{aligned}
\boldsymbol{\Phi}_{\theta_1} &= [0, \quad 0, \quad 1, \quad 0, \quad 0, \quad 0],\\
\boldsymbol{\Phi}_{\theta_2} &= [0, \quad 0, \quad 0, \quad 0, \quad 1, \quad 0],\\
\boldsymbol{\Phi}_{vx} &= [0, \quad 1, \quad 0, \quad 0, \quad 0 \quad , 0],\\
\boldsymbol{\Phi}_{v\theta_1} &= [0, \quad 0, \quad 0, \quad 1, \quad 0 \quad , 0],\\
\boldsymbol{\Phi}_{v\theta_2} &= [0, \quad 0, \quad 0, \quad 0, \quad 0 \quad , 1].
\end{aligned}$$

Then, with the purpose of transforming the problem in (17) into a convex optimization problem, we can alternatively rewrite the non-convex energy cost function in (16) into a convex form which will be given next.

Firstly, by inserting (4) into (16) and integrating the terms by parts, we have

$$\begin{aligned}
J =& \int_{\dot{x}(0)}^{\dot{x}(t_f)} (M + m_1 + m_2)\dot{x}\,\mathrm{d}\dot{x} + \int_{\dot{\theta}_1(0)}^{\dot{\theta}_1(t_f)} (m_1 + m_2)l_1\dot{x}\,\mathrm{d}\dot{\theta}_1 + \int_{\dot{\theta}_2(0)}^{\dot{\theta}_2(t_f)} m_2 l_2\dot{x}\,\mathrm{d}\dot{\theta}_2\\
=& C_1 - \int_0^{t_f} (m_1 + m_2)l_1\dot{\theta}_1\ddot{x}\mathrm{d}t - \int_0^{t_f} m_2 l_2\dot{\theta}_2\ddot{x}\mathrm{d}t.
\end{aligned} \tag{30}$$

Since t_f is a fixed termination time, $C_1 = \frac{1}{2}(M + m_1 + m_2)\dot{x}^2|_0^{t_f} + (m_1 + m_2)l_1\dot{x}\dot{\theta}_1|_0^{t_f} + m_2 l_2\dot{x}\dot{\theta}_2|_0^{t_f}$ is a constant. Further, $\ddot{x}$ can be eliminated by inserting (5) and (6) into (30) and derives

$$J = C_1 + C_2 + \int_0^{t_f} \left(d_1\dot{\theta}_1^2 + d_2\dot{\theta}_2^2\right). \tag{31}$$

Similarly, one can derive that $C_2 = \frac{1}{2}(m_1 + m_2)l_1^2\dot{\theta}_1^2|_0^{t_f} + \frac{1}{2}m_2 l_2^2\dot{\theta}_2^2|_0^{t_f} + \frac{1}{2}(m_1 + m_2)l_1 g\theta_1^2|_0^{t_f} + m_2 l_2 g\theta_2^2|_0^{t_f} + m_2 l_1 l_2\dot{\theta}_1\dot{\theta}_2|_0^{t_f}$. By using (13) and (14), one has that $C_1 = 0, C_2 = 0$. Then (31) becomes

$$J = \int_0^{t_f} \left(d_1\dot{\theta}_1^2 + d_2\dot{\theta}_2^2\right)\mathrm{d}t. \tag{32}$$

From (30)–(32), we can transform the problem of minimizing (16) into minimizing (32) equivalently, which is convex with respect to $\dot{\theta}_1(t)$ and $\dot{\theta}_2(t)$. Further, by discretization, we can convert the energy consumption (32) into the following form with respect to $\bar{\boldsymbol{u}}$:

$$\begin{aligned}
\bar{J} =& \sum_{k=0}^{k_f} \left[d_1\dot{\theta}_1^2(k) + d_2\dot{\theta}_2^2(k)\right]\tau\\
=& \left[d_1\|\dot{\boldsymbol{\theta}}_1\|_2^2 + d_2\|\dot{\boldsymbol{\theta}}_2\|_2^2\right]\tau\\
=& 2\left(\frac{1}{2}\bar{\boldsymbol{u}}^\top R\bar{\boldsymbol{u}} + \boldsymbol{r}^\top\bar{\boldsymbol{u}} + \varepsilon\right)\tau,
\end{aligned} \tag{33}$$

where (27) and (28) are used. The matrices $R \in \mathbb{R}^{k_f\times k_f}, \boldsymbol{r} \in \mathbb{R}^{k_f\times 1}$, and $\varepsilon \in \mathbb{R}$ in (33) are provided as follows:

$$\begin{aligned}
R &= Q^\top\left(d_1\Omega_{v\theta_1}^\top\Omega_{v\theta_1} + d_2\Omega_{v\theta_2}^\top\Omega_{v\theta_2}\right)Q,\\
\boldsymbol{r} &= Q^\top\left(d_1\Omega_{v\theta_1}^\top\Omega_{v\theta_1}P\boldsymbol{\chi}(0) + d_2\Omega_{v\theta_2}^\top\Omega_{v\theta_2}P\boldsymbol{\chi}(0)\right),\\
\varepsilon &= \frac{1}{2}\left(d_1\|\Omega_{v\theta_1}P\boldsymbol{\chi}(0)\|_2^2 + d_2\|\Omega_{v\theta_2}P\boldsymbol{\chi}(0)\|_2^2\right).
\end{aligned} \tag{34}$$

It can be seen from (33) that, the energy consumption satisfies the convexity condition.

Meanwhile, we discretize initial and final conditions shown in (13) and (14) by using (20) to obtain the following from with respect to $\bar{\boldsymbol{u}}$:

$$K\bar{\boldsymbol{u}} = \boldsymbol{k}, \tag{35}$$

where $K \in \mathbb{R}^{6\times k_f}$ and $\boldsymbol{k} \in \mathbb{R}^{6\times 1}$ are shown as follows:

$$K = \left[H^{k_f-1}\tau, \quad \cdots, \quad H^0\tau\right], \tag{36}$$

$$\boldsymbol{k} = \boldsymbol{\chi}(k_f) - H^{k_f}\boldsymbol{\chi}(0). \tag{37}$$

Additionally, based on (24)–(29), the state constraints of (15) can be written into the following discrete-time form with respect to $\bar{\boldsymbol{u}}$:

$$L\bar{\boldsymbol{u}} \preceq \boldsymbol{s}_1, L\bar{\boldsymbol{u}} \succeq \boldsymbol{s}_2, \tag{38}$$

where $L \in \mathbb{R}^{6k_f\times k_f}$ and $\boldsymbol{s}_1, \boldsymbol{s}_2 \in \mathbb{R}^{6k_f\times 1}$ have the following definitions:

$$L = \begin{bmatrix} \Omega_{vx}Q \\ \Omega_{\theta_1}Q \\ \Omega_{\theta_2}Q \\ \Omega_{v\theta_1}Q \\ \Omega_{v\theta_2}Q \\ I_{k_f} \end{bmatrix}, \tag{39}$$

$$\boldsymbol{s}_1 = \begin{bmatrix} v_{\max}\mathbf{1}^{k_f\times 1} - \Omega_{vx}P\boldsymbol{\chi}(0) \\ \theta_{1\max}\mathbf{1}^{k_f\times 1} - \Omega_{\theta_1}P\boldsymbol{\chi}(0) \\ \theta_{2\max}\mathbf{1}^{k_f\times 1} - \Omega_{\theta_2}P\boldsymbol{\chi}(0) \\ \theta_{1v\max}\mathbf{1}^{k_f\times 1} - \Omega_{v\theta_1}P\boldsymbol{\chi}(0) \\ \theta_{2v\max}\mathbf{1}^{k_f\times 1} - \Omega_{v\theta_2}P\boldsymbol{\chi}(0) \\ a_{\max}\mathbf{1}^{k_f\times 1} \end{bmatrix}, \tag{40}$$

$$\boldsymbol{s}_2 = \begin{bmatrix} -v_{\max}\mathbf{1}^{k_f\times 1} - \Omega_{vx}P\boldsymbol{\chi}(0) \\ -\theta_{1\max}\mathbf{1}^{k_f\times 1} - \Omega_{\theta_1}P\boldsymbol{\chi}(0) \\ -\theta_{2\max}\mathbf{1}^{k_f\times 1} - \Omega_{\theta_2}P\boldsymbol{\chi}(0) \\ -\theta_{1v\max}\mathbf{1}^{k_f\times 1} - \Omega_{v\theta_1}P\boldsymbol{\chi}(0) \\ -\theta_{2v\max}\mathbf{1}^{k_f\times 1} - \Omega_{v\theta_2}P\boldsymbol{\chi}(0) \\ -a_{\max}\mathbf{1}^{k_f\times 1} \end{bmatrix}, \tag{41}$$

where $\mathbf{1}^{k_f\times 1}$ denotes the $k_f \times 1$ column vector with all elements being identical to one.

After completing the discretization of the system dynamics, the energy consumption function, the initial/final conditions, and the state constraints, we can ultimately reformulate the problem in (17) into the following form:

$$\begin{aligned} \text{minimize } & \bar{J} = 2\left(\frac{1}{2}\bar{\boldsymbol{u}}^\top R\bar{\boldsymbol{u}} + \boldsymbol{r}^\top\bar{\boldsymbol{u}} + \varepsilon\right)\tau, \\ \text{s.t. } & K\bar{\boldsymbol{u}} = \boldsymbol{k}, \\ & L\bar{\boldsymbol{u}} \preceq \boldsymbol{s}_1, \\ & L\bar{\boldsymbol{u}} \succeq \boldsymbol{s}_2. \end{aligned} \tag{42}$$

Note that the problem shown in (42) is a QP problem with the convex objective function $\bar{J}$ shown in (33). Additionally, all the constraints are described in (38) which are affine with respect to the input sequence $\bar{\boldsymbol{u}}$. Then, we are admitted to use many convenient numerical solvers, e.g., the CVX (MATLAB software for disciplined convex programming), to find an optimal input sequence of this QP problem.

After that, from (20), the trajectories of positions and velocities will be obtained based on the proposed input sequence. Therefore, by applying the proposed energy-optimal trajectory planner, the energy-optimal trajectories for the displacements and velocities are generated, which can then be further implemented on the crane system to achieve the desired control objective.

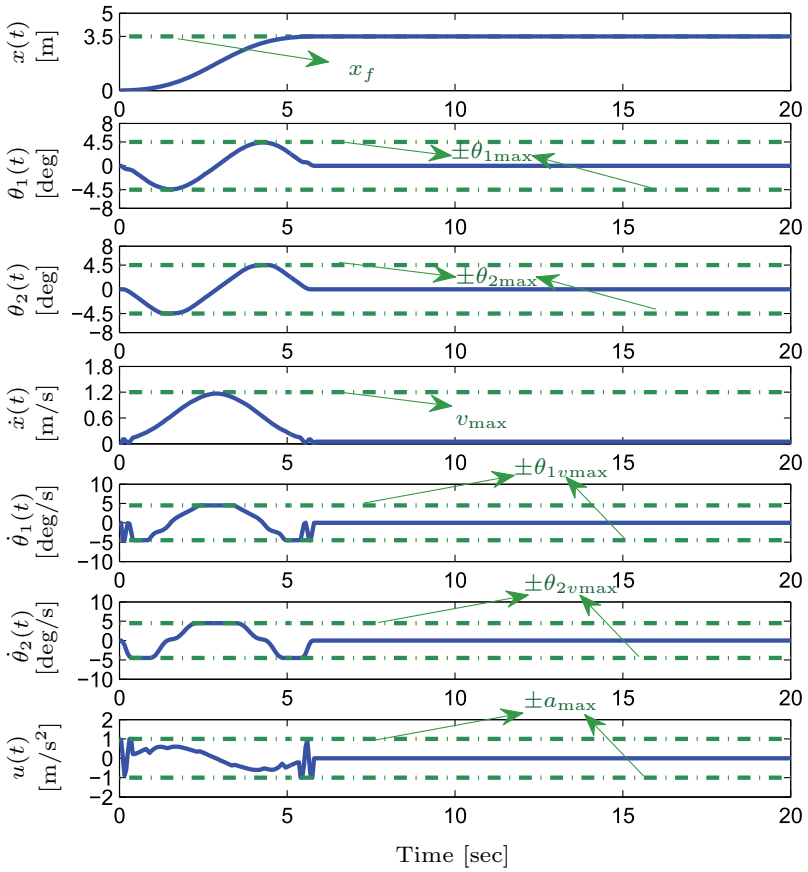

Fig. 2. The simulation results of the proposed planner in the situation of large industrial crane systems (green dot dashed lines: the boundaries of constraints in (45)). (For interpretation of the references to color in this figure legend, the reader is referred to the web version of this article.)

Remark 1. The linearization technique is a widely accepted way for trajectory planners, which is usually utilized to tackle high coupling and simplify mathematical analysis. Even though the system model is linearized, the double pendulum behavior still exists, which indicates that the linearized model can still describe the real behavior of double pendulum cranes with the small angle assumption. The results of simulation and experimental results will also indicate that the angles never escape the scope of constraints, which verifies the feasibility of linearization to a great extent.

Remark 2. The discretization of the system dynamics and state variables is reasonable. In either industrial or laboratory cranes, the sensor measured signals are discrete sequences, and the kernel control systems (DSP or PC) also implement the designed control algorithms in a discrete manner. In this sense, planning a discrete sequence trajectory, by using the control period as the discretization sampling time, is more convenient for practical applications.

Remark 3. The proposed energy-optimal problem is transformed into a QP problem which can be easily solved by using numerous numerical optimization solvers. Actually, it is enough to solve the proposed QP problem with only discrete numerical solution sequences, since the control algorithms are implemented in computer-based control systems, which provide discrete control commands.

Remark 4. The proposed open-loop trajectory planner is suitable in situations without severe perturbations. The robustness of the proposed open-loop method could be improved by being combined with some feedback tracking controllers with specific considerations on model uncertainty compensation. In this paper, together with the proposed energy-optimal planner, a common proportional-derivative (PD) controller is used and the control objectives is achieved satisfactorily. In our future work, more advanced controllers will be designed to enhance the robustness of the entire system.

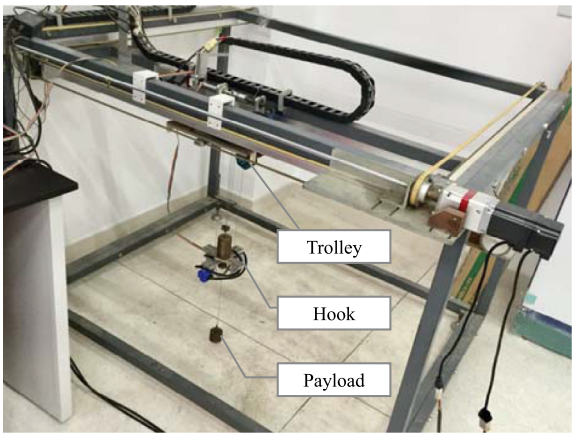

Fig. 3. The double pendulum crane hardware testbed.

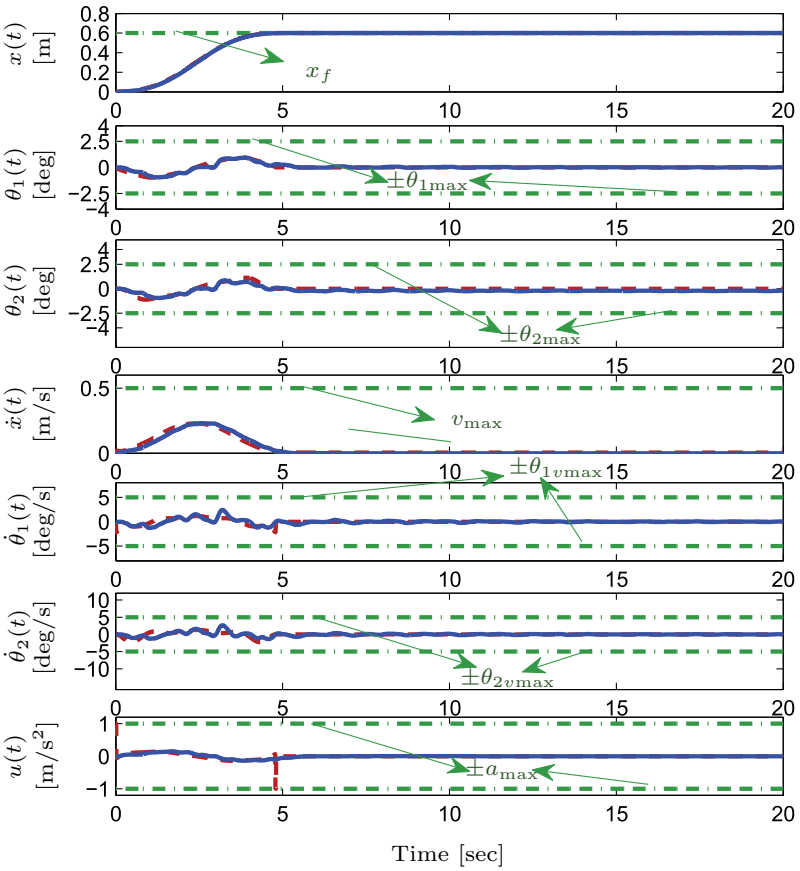

Fig. 4. The experimental results of the proposed planner with corresponding simulation results (blue solid lines: the experimental results; red dashed lines: the simulation results; green dot dashed lines: the boundaries of constraints in (49)). (For interpretation of the references to color in this figure legend, the reader is referred to the web version of this article.)

5. Simulation and hardware experiments

In this section, to illustrate the effectiveness of the proposed energy-optimal trajectory planner, some numerical simulation and hardware experimental results are provided. The optimization problem is solved by using the CVX optimization package in MATLAB. In addition, in the experiments, two existing effective controllers (the conventional sliding mode controller (CSMC) [46] and the linear quadratic regulator (LQR) based controller) are introduced as comparative methods. To be more intuitive, the angle unit is depicted as deg in the ensuing discussions [18].

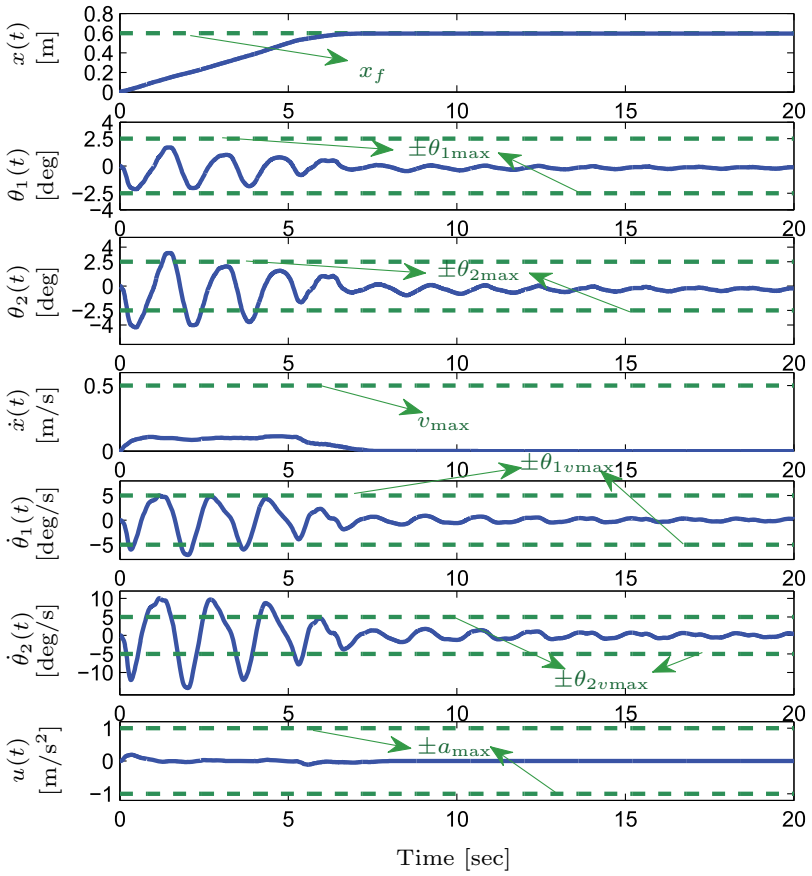

Fig. 5. The experimental results of the CSMC controller (green dashed lines: the boundaries of constraints in (49)). (For interpretation of the references to color in this figure legend, the reader is referred to the web version of this article.)

5.1. Numerical simulation

Due to the limited scale of the used hardware testbed, to test the performance in different system parameters, transportation distances, and damping conditions from the ensuing hardware experiments, the system parameters in this simulation test are set as follows:

$$\begin{aligned} &m_1 = 5\ \text{kg}, \quad m_2 = 5\ \text{kg}, \quad M = 10\ \text{kg}, \\ &l_1 = 1.2\ \text{m}, \quad l_2 = 0.4\ \text{m}, \quad g = 9.8\ \text{m/s}^2, \\ &d_1 = 0.12, \quad d_2 = 0.02, \end{aligned} \tag{43}$$

and the initial/final conditions are selected as follows:

$$\begin{aligned} &x_0 = 0\ \text{m}, \quad \theta_{10} = \theta_{20} = 0\ \text{deg}, \\ &\dot{x}_0 = 0\ \text{m/s}, \quad \dot{\theta}_{10} = \dot{\theta}_{20} = 0\ \text{deg/s}, \\ &x_f = 3.5\ \text{m}, \quad \theta_{1f} = \theta_{2f} = 0\ \text{deg}, \\ &\dot{x}_f = 0\ \text{m/s}, \quad \dot{\theta}_{1f} = \dot{\theta}_{2f} = 0\ \text{deg/s}. \end{aligned} \tag{44}$$

Additionally, the state constraints are

$$\begin{aligned} &a_{\max} = 1\ \text{m/s}^2, \quad v_{\max} = 1.2\ \text{m/s}, \\ &\theta_{1\max} = 4.5\ \text{deg}(i.e., 0.079\ \text{rad}), \quad \theta_{2\max} = 4.5\ \text{deg}(i.e., 0.079\ \text{rad}), \\ &\theta_{1v\max} = 4.5\ \text{deg/s}(i.e., 0.079\ \text{rad/s}), \quad \theta_{2v\max} = 4.5\ \text{deg/s}(i.e., 0.079\ \text{rad/s}). \end{aligned} \tag{45}$$

The sample time τ and the final sampling instant k_f are chosen as

$$\tau = 0.005\ \text{s}, \quad k_f = 1160, \tag{46}$$

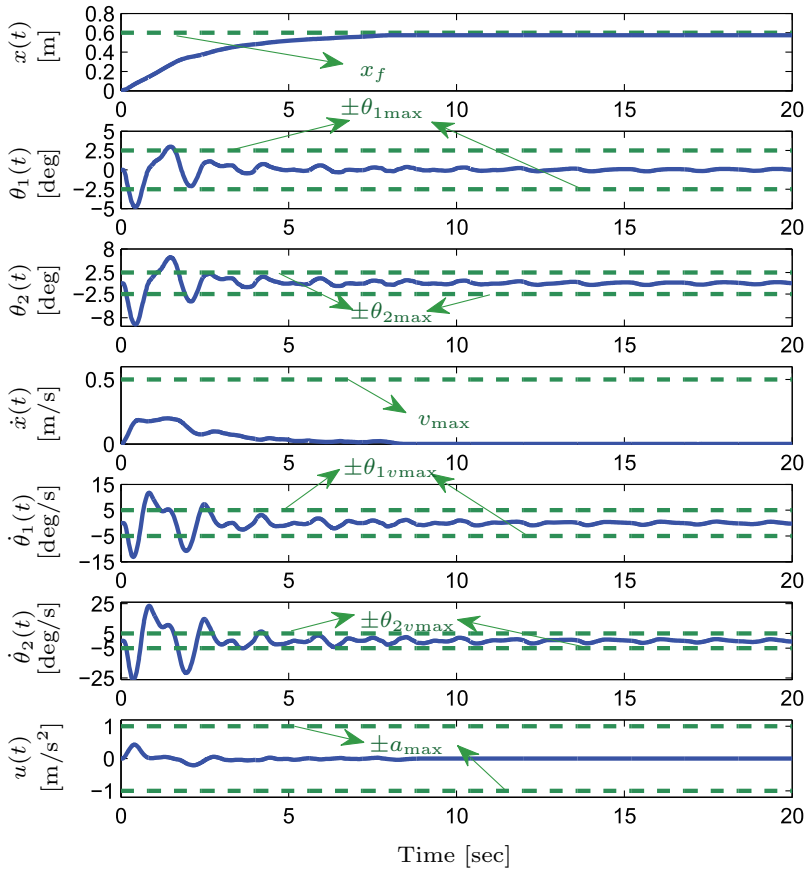

Fig. 6. The experimental results of the LQR controller (green dashed lines: the boundaries of state constraints in (49)). (For interpretation of the references to color in this figure legend, the reader is referred to the web version of this article.)

Table 2
Energy consumption comparison.

Planner/Controller	Cost Function [$\times 10^{-4}$ J]
The proposed planner	0.175
CSMC controller	4.485
LQR based controller	9.395

which indicates that the entire transportation task is expected to be completed within 5.8 s.

The simulation results are provided in Fig. 2. The simulation results show that during the entire transportation process, the position, the velocity and the input (acceleration) are all bounded within the constraints given in (45). More importantly, the trolley accurately reaches the desired location within 5.8 s, and there are no residual angle swings. These results are consistent with the theoretical analysis.

5.2. Hardware experiments

Further, to better validate the practical performance of the presented planner, some experiments are implemented on a self-built double pendulum crane hardware testbed. The experimental results are provided in Fig. 3 together with corresponding simulation results. The parameters of the hardware system are as follows:

$$\begin{aligned} &m_1 = 2.0\ \text{kg}, \quad m_2 = 0.5\ \text{kg}, \quad M = 6.5\ \text{kg}, \\ &l_1 = 0.53\ \text{m}, \quad l_2 = 0.4\ \text{m}, \quad g = 9.8\ \text{m/s}^2, \\ &d_1 = 0.013, \quad d_2 = 0.002, \end{aligned} \tag{47}$$

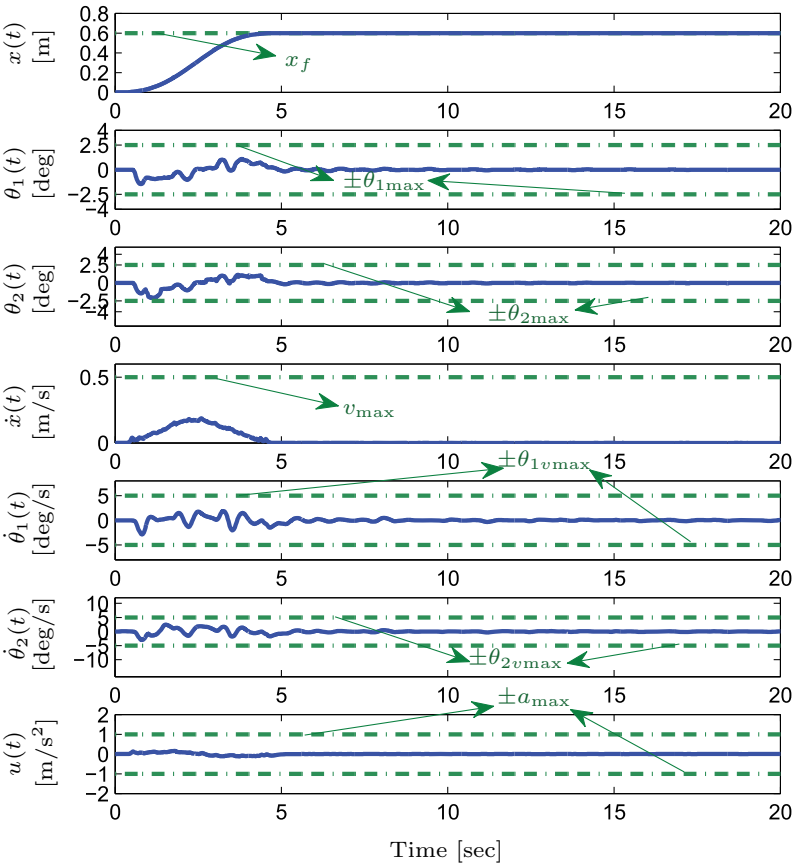

Fig. 7. The experimental results of the proposed planner when the rope length is given as 0.15 m.

where d_1 and d_2 are identified by off-line identification experiments.[2] For all the experiments, the initial/final conditions are given as follows:

$$\begin{aligned} &x_0 = 0\ \text{m}, \quad \theta_{10} = \theta_{20} = 0\ \text{deg},\\ &\dot{x}_0 = 0\ \text{m/s}, \quad \dot{\theta}_{10} = \dot{\theta}_{20} = 0\ \text{deg/s},\\ &x_f = 0.6\ \text{m}, \quad \theta_{1f} = \theta_{2f} = 0\ \text{deg},\\ &\dot{x}_f = 0\ \text{m/s}, \quad \dot{\theta}_{1f} = \dot{\theta}_{2f} = 0\ \text{deg/s}, \end{aligned} \tag{48}$$

and state constraints are

$$\begin{aligned} &a_{\max} = 1\ \text{m/s}^2, \quad v_{\max} = 0.5\ \text{m/s},\\ &\theta_{1\max} = 2.5\ \text{deg}(i.e., 0.044\ \text{rad}), \quad \theta_{2\max} = 2.5\ \text{deg}(i.e., 0.044\ \text{rad}),\\ &\theta_{1v\max} = 5\ \text{deg/s}(i.e., 0.087\ \text{rad/s}), \quad \theta_{2v\max} = 5\ \text{deg/s}(i.e., 0.087\ \text{rad/s}). \end{aligned} \tag{49}$$

The sample time τ and the final sampling instant k_f are

$$\tau = 0.005\ \text{s}, \quad k_f = 960, \tag{50}$$

which indicates that the entire transportation task is expected to be completed within 4.8 s. Associated with the proposed energy-optimal trajectories, a PD tracking control law is used. The driving force $u_0(t)$ is given as $u_0(t) = -k_p e_x(t) - k_d e_v(t)$, where $e_x(t), e_v(t)$ denote the tracking errors of the trolley position and velocity respectively, which are obtained by subtracting the proposed trajectories with expected destinations, and the control gains are given as $k_p = 150, k_d = 100$.

Additionally, two other controllers are introduced as comparative methods:

[2] In the experiments, the coefficients d_1 and d_2 are obtained by the following steps: (1) letting the payload swing freely; (2) recording the data/state trajectories (the positions and velocities); (3) identifying the coefficients d_1 and d_2 with the obtained experimental data.

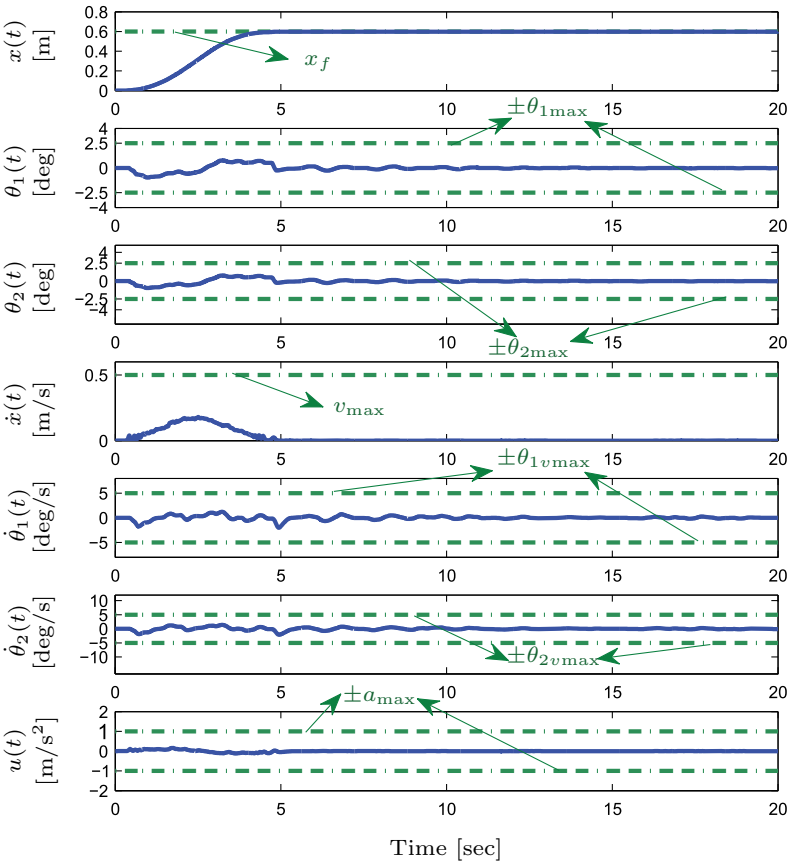

Fig. 8. The experimental results of the proposed planner when the rope length is given as 0.33 m.

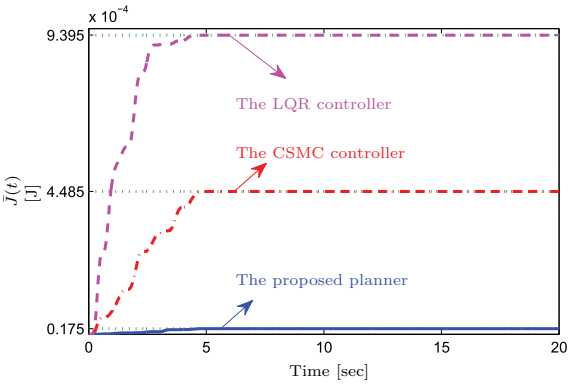

Fig. 9. The cost function of the optimization problem (42) (the blue solid line, red dot dashed line, and the purple dashed line denote $\bar{J}$ of the proposed planner, the CSMC, and the LQR controller, respectively). (For interpretation of the references to color in this figure legend, the reader is referred to the web version of this article.)

- A CSMC is introduced [46]. The trolley transportation movement is driven by the force $u_1(t)$ with the specific expression designed as $u_1(t) = -(m_1+m_2)l_1\cos\theta_1\ddot{\theta}_1 - m_2 l_2\cos\theta_2\ddot{\theta}_2 - (M+m_1+m_2)(\lambda\dot{x}+\alpha\dot{\theta}_1+\beta\dot{\theta}_2) - K_s\,\mathrm{sgn}(s)$, where s is the sliding surface defined as $s = \dot{x}+\lambda(x-x_f)+\alpha\theta_1+\beta\theta_2$, $\mathrm{sgn}(s)$ is the standard sign function, and the control gains are given as $\alpha = 1, \beta = -0.1, \lambda = 1, K_s = 10$.
- An LQR controller is introduced. By using MATLAB, the driving force $u_2(t)$ operating the trolley transportation movement can be obtained straightly as $u_2(t) = -K\boldsymbol{\chi}(t)$, where the control gain matrix K is given as $K = [48.99, 23.11, -49.59, 1.97, 7.95, -2.49]$.

The experimental results are shown in Figs. 4–6. In particular, in Fig. 4, together with the experimental results (the blue solid lines), the corresponding simulation results (using the same parameters and conditions) are also provided by red dashed lines. The comparison of the blue solid lines and the red dashed lines in Fig. 4 verifies that the experimental results are consistent with the simulation results in general. Specifically, as seen from Fig. 4, all the state variables are limited in the scope of the state constraints in (49), which are drawn with green horizontal dot dashed lines. The trolley reaches the desired location rapidly and accurately, and there are almost no residual swing motions. Therefore, the proposed planner achieves the control objective and satisfactorily ensures the physical constraints, including maximum velocity, acceleration, and swing amplitudes. Figs. 5 and 6 show the results of the comparative CSMC and LQR controller.[3] Specifically, in Fig. 5, the trolley reaches the same desired location within about 7 s, which is slower than the proposed planner. In addition, the payload swings more severely, which may bring safety concerns ($\theta_2(t), \dot{\theta}_1(t), \dot{\theta}_2(t)$ all exceed the given constraints). For example, in Fig. 5, the largest amplitude of $\dot{\theta}_2(t)$ reaches over 10 deg/s but in Fig. 4 the amplitude of $\dot{\theta}_2(t)$ never exceeds 5 deg/s. Meanwhile, there still exist residual oscillations in Fig. 5. Similarly, in Fig. 6, the LQR controller results in much larger angle amplitudes (the largest amplitude of $\dot{\theta}_2(t)$ reaches about 25 deg/s) and also fails to suppress residual oscillations. In summary, both comparative methods fail to suppress the residual oscillations effectively. In general, compared with the results of the CSMC and LQR controllers shown in Figs. 5 and 6, the presented planner in Fig. 4 gives better performance in the following aspects: (1) It can make the system achieve the desired position with all the constraints being restricted within the given scope in (49). (2) It can suppress the residual swing effectively. (3) It consumes less energy than the comparative methods, with a smaller $\bar{J}$ in (42) as shown in Fig. 9 and Table 2. (4) It takes less time to finish the transportation control tack (since both of the comparative methods take about 5–10 s to achieve the control task, for the experiments of the proposed energy-optimal trajectory planner shown in Fig. 4, a shorter termination time is determined as 4.8 s). These results demonstrate the efficiency and feasibility of the proposed planner.

Then, we further test the performance of the proposed planner for different rope lengths. To this end, the rope length is adjusted as 0.15 m and 0.33 m, respectively. The trajectories corresponding to the new rope lengths are planned conveniently, while the other system parameters and initial/final conditions are kept the same as before. The experimental results are provided in Figs. 7 and 8, which show that, with different rope lengths, the proposed trajectories can achieve the control objectives with all state variables being constrained within given scopes and residual swings being eliminated effectively.

6. Conclusion

An energy-optimal trajectory planner has been presented for double pendulum crane systems with various state constraints. Based on the convexification of the energy consumption function and the discretization of the system dynamics, the energy consumption, the initial/final conditions, and the state constraints, the control problem is elaborately reformulated into a QP problem, whose solution is then obtained by using a convex optimization tool. Both numerical simulation and hardware experimental results are provided. The proposed planner can minimize the system energy cost and respect the physical constraints as well. Additionally, as verified by hardware experiments, the proposed scheme can achieve superior control performance over the comparative methods in terms of fast trolley positioning, smaller swing amplitudes, and less energy consumption.

Acknowledgement

We would like to sincerely acknowledge the reviewers and the Associate Editor for the valuable comments/suggestions, which are very helpful for this paper's improvement. This work is supported by the National Natural Science Foundation of China under Grant 61503200, the Natural Science Foundation of Tianjin under Grant 15JCQNJC03800, the China Postdoctoral Science Foundation under Grants 2016M600186 and 2017T100153, and the Fundamental Research Funds for the Central Universities. Ning Sun and Yiming Wu contributed equally to this paper.

References

[1] P. Olejnik, J. Awrejcewicz, Coupled oscillators in identification of nonlinear damping of a real parametric pendulum, Mech. Syst. Signal Process. 98 (2018) 91–107.
[2] X. Sun, X. Jing, A nonlinear vibration isolator achieving high-static-low-dynamic stiffness and tunable anti-resonance frequency band, Mech. Syst. Signal Process. 80 (2016) 166–188.
[3] X. Sun, X. Jing, Analysis and design of a nonlinear stiffness and damping system with a scissor-like structure, Mech. Syst. Signal Process. 66–67 (2016) 723–742.
[4] L. Edalati, A.K. Sedigh, M.A. Shooredeli, A. Moarefianpour, Adaptive fuzzy dynamic surface control of nonlinear systems with input saturation and time-varying output constraints, Mech. Syst. Signal Process. 100 (2018) 311–329.
[5] X. Kong, X. Zhang, X. Chen, B. Wen, B. Wang, Synchronization analysis and control of three eccentric rotors in a vibrating system using adaptive sliding mode control algorithm, Mech. Syst. Signal Process. 72–73 (2016) 432–450.

[3] The green dashed lines in Figs. 4–6 denote the same constraint boundaries in (49), except that the ranges of the vertical axes of θ_1 and θ_2 of Fig. 6 are larger than those of the other two.

[6] D. Richiedei, A. Trevisani, Simultaneous active and passive control for eigenstructure assignment in lightly damped systems, Mech. Syst. Signal Process. 85 (2017) 556–566.
[7] B. Sumantri, N. Uchiyama, S. Sano, Least square based sliding mode control for a quad-rotor helicopter and energy saving by chattering reduction, Mech. Syst. Signal Process. 66–67 (2016) 769–784.
[8] H. Pan, X. Jing, W. Sun, Robust finite-time tracking control for nonlinear suspension systems via disturbance compensation, Mech. Syst. Signal Process. 88 (2017) 49–61.
[9] X. Xin, Y. Liu, Reduced-order stable controllers for two-link underactuated planar robots, Automatica 49 (7) (2013) 2176–2183.
[10] C. Yang, Z. Li, J. Li, Trajectory planning and optimized adaptive control for a class of wheeled inverted pendulum vehicle models, IEEE Trans. Cybernet. 43 (1) (2013) 24–36.
[11] N. Sun, Y. Wu, Y. Fang, H. Chen, B. Lu, Nonlinear continuous global stabilization control for underactuated RTAC systems: design, analysis, and experimentation, IEEE/ASME Trans. Mech. 22 (2) (2017) 1104–1115.
[12] H. Chen, M. Zhang, H. Mu, Y. Zhu, C. Hu, T. Cai, Conceptual design and trajectory planning of a precision repetitive-scanning stage with separated drive unit for energy saving, IEEE/ASME Trans. Mech. 21 (4) (2016) 2142–2153.
[13] C. Yang, Z. Li, R. Cui, B. Xu, Neural network-based motion control of an underactuated wheeled inverted pendulum models, IEEE Trans. Neural Netw. Learn. Syst. 25 (11) (2014) 2004–2016.
[14] N. Sun, Y. Wu, Y. Fang, H. Chen, Nonlinear stabilization control of multiple-RTAC systems subject to amplitude-restricted actuating torques using only angular position feedback, IEEE Trans. Industr. Electron. 64 (4) (2017) 3084–3094.
[15] L. Ramli, Z. Mohamed, A.M. Abdullahi, H.I. Jaafar, I.M. Lazim, Control strategies for crane systems: a comprehensive review, Mech. Syst. Signal Process. 95 (2017) 1–23.
[16] L.A. Tuan, S.-G. Lee, S.-C. Moon, Partial feedback linearization and sliding mode techniques for 2D crane control, Trans. Inst. Meas. Contr. 36 (1) (2014) 78–87.
[17] W. He, S. Zhang, S.S. Ge, Adaptive control of a flexible crane system with the boundary output constraint, IEEE Trans. Industr. Electron. 61 (8) (2014) 4126–4133.
[18] M. Zhang, X. Ma, X. Rong, X. Tian, Y. Li, Error tracking control for underactuated overhead cranes against arbitrary initial payload swing angles, Mech. Syst. Signal Process. 84 (A) (2017) 268–285.
[19] Z. Zhang, Y. Wu, J. Huang, Differential-flatness-based finite-time anti-swing control of underactuated crane systems, Nonlinear Dyn. 87 (3) (2017) 1749–1761.
[20] Q.H. Ngo, K.-S. Hong, Sliding-mode antisway control of an offshore container crane, IEEE/ASME Trans. Mech. 17 (2) (2012) 201–209.
[21] H.-H. Lee, Y. Liang, D. Segura, A sliding-mode antiswing trajectory control for overhead cranes with high-speed load hoisting, J. Dyn. Syst. Meas. Contr. 128 (4) (2006) 842–845.
[22] D. Qian, J. Yi, Design of combining sliding mode controller for overhead crane systems, Int. J. Contr. Automat. 6 (1) (2013) 131–140.
[23] N. Sun, Y. Fang, H. Chen, Y. Fu, B. Lu, Nonlinear stabilizing control for ship-mounted cranes with disturbances with ship roll and heave movements: design, analysis, and experiments. IEEE Trans. Syst. Man Cybernet.: Syst. [in press]. http://dx.doi.org/10.1109/TSMC.2017.2700393.
[24] N. Sun, Y. Fang, H. Chen, Y. Wu, B. Lu, Nonlinear antiswing control of offshore cranes with unknown parameters and persistent ship-induced perturbations: theoretical design and hardware experiments. IEEE Trans. Industr. Electron [in press].
[25] N. Sun, Y. Wu, Y. Fang, and H. Chen, Nonlinear antiswing control for crane systems with double pendulum swing effects and uncertain parameters: design and experiments. IEEE Trans. Automat. Sci. Eng. http://dx.doi.org/10.1109/TASE.2017.2723539 [in press].
[26] M. Volckaert, M. Diehl, J. Swevers, Generalization of norm optimal ILC for nonlinear systems with constraints, Mech. Syst. Signal Process. 39 (1–2) (2013) 280–296.
[27] J. Smoczek, Experimental verification of a GPC-LPV method with RLS and P1-TS fuzzy-based estimation for limiting the transient and residual vibration of a crane system, Mech. Syst. Signal Process. 62–63 (2015) 324–340.
[28] Y. Zhao, H. Gao, Fuzzy-model-based control of an overhead crane with input delay and actuator saturation, IEEE Trans. Fuzzy Syst. 20 (1) (2012) 181–186.
[29] W. Yu, M.A. Moreno-Armendariz, F.O. Rodriguez, Stable adaptive compensation with fuzzy CMAC for an overhead crane, Informat. Sci. 181 (21) (2011) 4895–4907.
[30] B. Käpernick, K. Graichen, Model predictive control of an overhead crane using constraint substitution, in: American Control Conference (ACC), Washington, DC, USA, 2013, pp. 3973–3978.
[31] R. Toxqui, W. Yu, X. Li, Anti-swing control for overhead crane with neural compensation, in: International Joint Conference on Neural Networks, Vancouver, BC, Canada, 2006, pp. 4697–4703.
[32] S.C. Duong, E. Uezato, H. Kinjo, T. Yamamoto, A hybrid evolutionary algorithm for recurrent neural network control of a three-dimensional tower crane, Automat. Constr. 23 (2012) 55–63.
[33] N. Sun, Y. Fang, X. Zhang, Y. Yuan, Transportation task-oriented trajectory planning for underactuated overhead cranes using geometric analysis, IET Contr. Theor. Appl. 6 (10) (2012) 1410–1423.
[34] N. Sun, Y. Fang, Y. Zhang, B. Ma, A novel kinematic coupling-based trajectory planning method for overhead cranes, IEEE/ASME Trans. Mech. 17 (1) (2012) 166–173.
[35] Z. Wu, X. Xia, Optimal motion planning for overhead cranes, IET Contr. Theor. Appl. 8 (17) (2014) 1833–1842.
[36] X. Xie, J. Huang, Z. Liang, Vibration reduction for flexible systems by command smoothing, Mech. Syst. Signal Process. 39 (1–2) (2013) 461–470.
[37] M.J. Maghsoudi, Z. Mohamed, S. Sudin, S. Buyamin, H.I. Jaafar, S.M. Ahmad, An improved input shaping design for an efficient sway control of a nonlinear 3D overhead crane with friction, Mech. Syst. Signal Process. 92 (2017) 364–378.
[38] D. Fujioka and W. Singhose, Control effort reduction analysis of zero-vibration model reference control for controlling a time-varying plant, in: American Control Conference (ACC), Portland, Oregon, USA, 2014, pp. 3110–3115.
[39] M.J. Maghsoudi, Z. Mohamed, A.R. Husain, M.O. Tokhi, An optimal performance control scheme for a 3D crane, Mech. Syst. Signal Process. 66–67 (2016) 756–768.
[40] M. Zhang, X. Ma, X. Rong, X. Tian, Y. Li, Adaptive tracking control for double-pendulum overhead cranes subject to tracking error limitation, parametric uncertainties and external disturbances, Mech. Syst. Signal Process. 76–77 (2016) 15–32.
[41] J. Vaughan, D. Kim, W. Singhose, Control of tower cranes with double-pendulum payload dynamics, IEEE Trans. Contr. Syst. Technol. 18 (6) (2010) 1345–1358.
[42] J. Huang, Z. Liang, Q. Zang, Dynamics and swing control of double-pendulum bridge cranes with distributed-mass beams, Mech. Syst. Signal Process. 54–55 (2015) 357–366.
[43] D. Fujioka, W. Singhose, Performance comparison of input-shaped model reference control on an uncertain flexible system, Int. Fed. Autom. Contr. (IFAC) – PapersOnLine 48 (12) (2015) 129–134.
[44] Z. Masoud, K. Alhazza, E. Abu-Nada, M. Majeed, A hybrid command-shaper for double-pendulum overhead cranes, J. Vib. Contr. 20 (1) (2014) 24–37.
[45] K.-T. Hong, C.-D. Huh, K.-S. Hong, Command shaping control for limiting the transient sway angle of crane systems, Int. J. Contr. Autom. Syst. 1 (1) (2003) 43–53.
[46] L.A. Tuan, S.-G. Lee, Sliding mode controls of double-pendulum crane systems, J. Mech. Sci. Technol. 27 (6) (2013) 1863–1873.
[47] D. Liu, W. Guo, J. Yi, Dynamics and GA-based stable control for a class of underactuated mechanical systems, Int. J. Contr. Autom. Syst. 6 (1) (2008) 35–43.
[48] D. Qian, S. Tong, S.G. Lee, Fuzzy-logic-based control of payloads subjected to double-pendulum motion in overhead cranes, Automat. Constr. 65 (2016) 133–143.
[49] N. Sun, Y. Fang, H. Chen, B. Lu, Amplitude-saturated nonlinear output feedback antiswing control for underactuated cranes with double-pendulum cargo dynamics, IEEE Trans. Industr. Electron. 64 (3) (2017) 2135–2146.